

# Practical advantage of non-Hermitian enhanced quantum sensing

Kun Yang,<sup>1,2</sup> Yaoming Chu,<sup>1,2,\*</sup> Ning Wang,<sup>1,2,†</sup> and Jianming Cai<sup>1,2</sup>

<sup>1</sup>*School of Physics, Center for Intelligence and Quantum Science (CIQS),  
International Joint Laboratory on Quantum Sensing and Quantum Metrology,  
Huazhong University of Science and Technology, Wuhan, 430074, China*

<sup>2</sup>*Hubei Key Laboratory of Gravitation and Quantum Physics, Institute for Quantum Science and Engineering,  
Huazhong University of Science and Technology, Wuhan, 430074, China*

Non-Hermitian systems have emerged as a powerful paradigm for ultrasensitive sensing, leveraging unique spectral and dynamical properties that find no counterparts in Hermitian physics. While recent theoretical assessments have established that these protocols offer no fundamental advantage in the ideal shot-noise-limited regime once the success probability of non-unitary evolution is rigorously accounted for, their practical utility under realistic experimental constraints remains largely unexplored. In this work, we shift the focus toward practical laboratory performance by demonstrating that non-Hermitian sensors can significantly outperform their Hermitian counterparts in the presence of various types of technical noise. This enhancement stems from the significantly enhanced susceptibility, which amplifies the signal response to effectively overcome the floor of technical imperfections. By evaluating the Fisher information under different technical noise models, we further substantiate the superior performance of non-Hermitian sensing. Our results delineate the specific regimes where non-Hermitian platforms yield clear practical gains, offering a concrete avenue for building high-precision, noise-resilient sensors.

## I. INTRODUCTION

The study of non-Hermitian systems has rapidly evolved into a vibrant interdisciplinary frontier, fundamentally reshaping our understanding of open quantum dynamics and wave phenomena [1–3]. A seminal milestone was the discovery by Bender and Boettcher that non-Hermitian Hamiltonians—most notably those respecting parity-time ( $\mathcal{PT}$ ) symmetry—can possess entirely real spectra symmetry [4–7]. This finding challenged the long-held axiom that Hermiticity is a prerequisite for physical observables, thereby catalyzing new avenues in both foundational theory and experimental exploration [8–10].

At the heart of these developments lies the existence of exceptional points (EPs): non-Hermitian degeneracies where both eigenvalues and eigenvectors simultaneously coalesce, leading to a collapse of the underlying Hilbert space dimensionality [11–13]. In the vicinity of an  $n$ th-order EP, a weak perturbation of strength  $\epsilon$  induces a singular spectral response scaling as  $\epsilon^{1/n}$  [14, 15]. This unconventional scaling, which formally diverges in the limit of vanishing perturbations, has motivated a surge of interest in EP-enhanced sensing protocols. Successful experimental realizations have spanned a diverse range of macroscopic coupled-mode models, including optical systems [16–25], electric circuits [26–28], mechanical systems [29, 30], and microresonators [31–37].

However, it has been increasingly recognized that translating this radical spectral response into improved metrological precision faces fundamental hurdles specific

to the EP physics [13, 15, 38–45]. A fundamental bottleneck specific to EP-based sensing stems from the simultaneous coalescence of eigenvectors: as the eigenmodes become nearly parallel, the distinguishability of physical states is severely degraded, potentially neutralizing the gains in susceptibility [13, 46]. In dissipative optical systems and laser-based gyroscopes, this manifests as an excess noise enhancement—where the non-orthogonality of eigenmodes amplifies the coupling of stochastic fluctuations (such as spontaneous emission) into the lasing mode and leads to a dramatic broadening of the spectral linewidth beyond the standard Schawlow-Townes limit. This phenomenon is formally quantified by the Petermann factor  $K$  [13, 15, 47, 48]. As the system approaches an  $n$ th-order EP, the Petermann factor diverges as  $K \propto \epsilon^{-2(n-1)/n}$ , effectively neutralizing the sensitivity gain and restoring the linear scaling of the overall signal-to-noise ratio. Furthermore, when implemented in genuine quantum sensors—such as solid-state spins [49], dissipative ultracold atoms [50], superconducting qubits [51]—one encounters a temporal resource constraint. To effectively resolve the singular energy splitting  $\Delta E \sim \epsilon^{1/n}$  near an EP, the required interrogation time  $T$  must scale as  $1/\Delta E$ , leading to a critical slowing down that causes the measurement time to diverge. Meanwhile, the experimental realization of an EP remains highly demanding, as it requires the exquisite fine-tuning of system parameters—such as the delicate balance of dissipation rates against coherent coupling and the precise calibration of driving field intensities—to stabilize the system within the non-Hermitian critical regime.

To circumvent these fundamental and operational constraints—specifically the temporal limitations and the stringent requirements for experimental stabilization—the field has recently expanded into broader non-

---

\* yaomingchu@hust.edu.cn

† ningwang@hust.edu.cn

Hermitian paradigms. One prominent direction involves non-Hermitian quantum dynamics, which exploits intrinsic features such as complex-valued spectra and eigenstate non-orthogonality in the absence of EPs [41, 52–54]. By operating away from the degeneracy points, these dynamical protocols aim to enhance precision without suffering from critical slowing down. In parallel, non-Hermitian topology has emerged as another robust alternative, where phenomena such as the non-Hermitian skin effect leverage the extreme sensitivity of the bulk spectrum to boundary conditions, offering a radical departure from the localized sensing paradigms of Hermitian physics [27, 28, 36, 55].

Despite the diversity of these strategies, the physical realization of non-Hermiticity remains a nontrivial task, as closed quantum systems are strictly governed by Hermitian Hamiltonians. One established route is through open quantum systems effectively described by the master equation [56, 57]. In the quantum-trajectory picture, conditioning the dynamics on the absence of quantum jumps reduces the evolution to that governed by an effective non-Hermitian Hamiltonian. Nevertheless, this approach is severely limited by a success probability that decays exponentially with time; moreover, the accurate and efficient identification of null-emission events poses strict challenges for experiments. A more robust alternative involves engineering target non-Hermitian dynamics within an enlarged Hermitian framework by leveraging postselection techniques [58, 59]. Yet, both approaches are ultimately hindered by the diminishing success probability of postselection. Once this probability is rigorously incorporated into the resource accounting, non-Hermitian sensors often show no fundamental advantage over their Hermitian counterparts, particularly from the perspective of quantum Fisher information [54, 60, 61].

Such a fundamental assessment, however, assumes an idealized environment where precision is solely governed by intrinsic quantum fluctuations. In practical laboratory settings, however, the performance ceiling is often redefined by technical imperfections rather than fundamental limits. This leads to a pivotal question: does the absence of a universal quantum advantage preclude the practical utility of non-Hermitian sensing in the real world? While previous critiques have focused on fundamental limits like shot noise, the impact of technical noise sources—such as readout noise, systematic calibration errors, and detector saturation—remains a critical missing link. In many experimental settings, these technical imperfections define the operational ceiling of the sensor. Understanding how non-Hermiticity reconfigures the system’s response to these practical constraints is essential for determining whether such devices can transition from theoretical curiosities to functional quantum technologies.

In this work, we address this gap by providing a comprehensive analysis of non-Hermitian sensing under various realistic technical noises. We demonstrate that while non-Hermitian protocols may not provide a universal ad-

vantage in the ideal limit, they offer substantial noise-resilience in regimes where errors cannot be efficiently suppressed by simple averaging over repetitive measurements. We also establish an information-theoretic framework based on Fisher information to identify the operational boundaries where non-Hermitian sensors demonstrate clear metrological gains. Our results provide a concrete roadmap for the implementation of noise-resilient, non-Hermitian quantum technologies.

The paper is organized as follows. In Sect. II, we introduce mechanisms of non-Hermitian sensing, highlighting the differences between EP-based and universal non-Hermitian approaches as well as the comparison to the Hermitian counterparts. In Sec. III, we explicitly investigate the impact of various technical noise on the measurement precision of non-Hermitian sensing. Section IV develops an information-theoretic perspective through quantum and classical Fisher information. Finally, Sec. V summarizes our findings and discusses the implications for experimental realization.

## II. NON-HERMITIAN SENSING

### A. Exceptional-point (EP) based sensing

The use of non-Hermitian physics for quantum sensing can be traced back to the discovery that macroscopic coupled-mode systems operating near an exceptional point (EP) exhibit an anomalously amplified response to weak external perturbations. This behavior sharply contrasts with that of Hermitian systems, where eigenvalue splittings scale linearly with the perturbation strength near ordinary degeneracies [62, 63]. The response enhancement near an EP arises from the coalescence of both eigenvalues and eigenvectors—a feature unique to non-Hermitian degeneracies—which gives rise to non-analytic spectral responses.

To grasp the essential mechanism underlying this enhancement, it is instructive to examine a minimal two-level non-Hermitian Hamiltonian,

$$H_0 = \begin{pmatrix} 0 & A \\ A' & 0 \end{pmatrix}, \quad (1)$$

where  $A$  and  $A'$  are taken to be real parameters. This simple model already captures the qualitative distinction between Hermitian and non-Hermitian behavior. When  $A = A'$ , the Hamiltonian is Hermitian, and the two eigenmodes remain orthogonal. When  $A \neq A'$ , the system becomes non-Hermitian and the eigenmodes lose orthogonality, ultimately coalescing into a single defective state at the EP. In either case, the unperturbed eigenenergies meet at  $E = 0$ , but the structure of the degeneracy is fundamentally different. To probe how these two scenarios respond to weak external perturbations, we introduce

a small symmetric coupling of strength  $\lambda$ ,

$$H = H_0 + H', \quad H' = \begin{pmatrix} 0 & \lambda \\ \lambda & 0 \end{pmatrix}, \quad (2)$$

and examine the resulting spectral splitting. For small  $\epsilon$ , the behaviour is strikingly different in the Hermitian and non-Hermitian regimes:

$$\Delta E_H \simeq \lambda, \quad (3)$$

$$\Delta E_{nH} \simeq \sqrt{\lambda}. \quad (4)$$

The Hermitian case exhibits the expected linear response of first-order perturbation theory, whereas at the second-order EP the square-root dependence reveals the characteristic branch-point structure of non-Hermitian degeneracies. More broadly, an EP of order  $n$  produces an eigenvalue splitting that scales as  $\epsilon^{1/n}$  for perturbation  $\epsilon$ , implying an increasingly amplified sensitivity to weak perturbations as the EP order increases. This striking scaling has inspired numerous theoretical proposals and experimental demonstrations aiming to exploit EPs for enhanced sensing beyond conventional limits [14, 15].

Here we focus on EP-based sensing in single quantum systems. Consider a single-qubit dissipative system described by the following Hamiltonian,

$$\hat{H}_0 = J\hat{\sigma}_x - i\frac{\Gamma}{2}\hat{\sigma}_z - i\frac{\Gamma}{2}\hat{\mathbb{I}}, \quad (5)$$

where  $\hat{\sigma}_{x,z}$  are the Pauli operators,  $\hat{\mathbb{I}}$  represents the density operator. When neglecting the last global decay term, Eq. (5) can be viewed as a PT-symmetric Hamiltonian and exhibits a second-order EP at  $J = \Gamma/2$ . Now we assume that a perturbation term of  $\hat{H}_s = \lambda\sigma_z$  that emulates a weak signal is added. The corresponding spectral splitting, i.e.  $\Omega = [J^2 + (\lambda - i\Gamma/2)^2]^{1/2}$  can be determined through

$$P_J(T) + P_\Gamma(T) = e^{-\Gamma T} |\sin(\Omega T)|^2, \quad (6)$$

where

$$\begin{aligned} P_J(T) &= |\langle \uparrow | U(T) | \downarrow \rangle|^2, \\ P_\Gamma(T) &= |\langle - | U(T) | + \rangle|^2, \end{aligned} \quad (7)$$

are two measurable quantities in experiments with  $U(T) = \exp[-i(\hat{H}_0 + \hat{H}_s)T]$  and  $|\pm\rangle = (|\uparrow\rangle \pm |\downarrow\rangle)/\sqrt{2}$ .

However, one must be cautious in interpreting the enhanced spectral response near an EP as a guaranteed metrological advantage [13, 46]. In the above protocol, the effective detection of  $\Omega$  also requires a diverging time to ensure  $\Omega T \sim O(1)$  as  $\lambda \rightarrow 0$  in the vicinity of EP, which is indeed an impractical regime in real sensing process and suffers from severe decoherence effect. Next we present a more general method which does not depend on EP and non-Hermitian criticality can be accessed at finite evolution time.

## B. General non-Hermitian sensing framework

Transcending conventional EP-based sensing schemes, generic non-Hermitian dynamics can also significantly enhance the susceptibility of a quantum system to weak perturbations. To illustrate such a universal mechanism, we consider a single-qubit non-Hermitian Hamiltonian denoted by  $H_0$ . The eigenvectors of  $H_0$  are generally non-orthogonal, and can be expressed as

$$\begin{aligned} |\psi_+\rangle &\sim |0\rangle + \delta|1\rangle, \\ |\psi_-\rangle &\sim |0\rangle - (\delta/a)|1\rangle, \end{aligned} \quad (8)$$

where  $a, \delta \in \mathbb{C}$  and  $|a| \leq 1$ . Here,  $\delta$  characterizes the deviation from the computational basis state  $|0\rangle$ , and  $a$  controls the overlap between  $|\psi_\pm\rangle$ . By assuming the two associated eigenvalues as  $\mathcal{E}_+$  and  $\mathcal{E}_-$ , the Hamiltonian takes the explicit form

$$H_0 = \frac{\mathcal{E}_+ - \mathcal{E}_-}{1+a} \begin{pmatrix} 1 & \frac{a}{\delta} \\ \delta & a \end{pmatrix} + \mathcal{E}_- I. \quad (9)$$

Without loss of generality, we set  $\mathcal{E}_+ = 2\mathcal{E} \in \mathbb{C}$  and  $\mathcal{E}_- = 0$  in the following.

Next, we proceed to consider such a non-Hermitian qubit system as sensor perturbed by an external weak signal  $\lambda V$  [41], where  $\lambda$  represents the unknown parameter to be estimated; the corresponding total Hamiltonian thereby reads,

$$H = H_0 + \lambda V. \quad (10)$$

For concreteness, we set  $V = \sigma_x$ . We point out that the eigenvectors of  $H$  can still be expressed as the general form of Eq. (8), but with the parameters  $\{\delta, a, \mathcal{E}\}$  implicitly depending on  $\lambda$  hereafter. Starting from the initial state  $|\psi(0)\rangle = |0\rangle$ , the time-evolved state is given by

$$\begin{aligned} |\psi(t)\rangle &= e^{-iHt} |\psi(0)\rangle \\ &= \frac{1 - e^{i2\mathcal{E}t}}{1+a} (\mathcal{D}_t |0\rangle + \delta |1\rangle) \end{aligned} \quad (11)$$

where  $\mathcal{D}_t$  determines the amplitude of the initial state during evolution

$$2\mathcal{D}_t = (1-a) + i(1+a) \cot(\mathcal{E}t). \quad (12)$$

Immediately, the probability of obtaining a measurement outcome  $|0\rangle$  is given by

$$p_{nH}(t, \lambda) = \frac{|\mathcal{D}_t|^2}{|\delta|^2 + |\mathcal{D}_t|^2}, \quad (13)$$

Its sensitivity to  $\lambda$  is characterized by

$$\chi_{nH}(\lambda) \equiv \left| \frac{\partial p_{nH}(t, \lambda)}{\partial \lambda} \right| = \chi_{|\delta|} \frac{\partial |\delta|}{\partial \lambda} + \chi_{|\mathcal{D}_t|} \frac{\partial |\mathcal{D}_t|}{\partial \lambda}, \quad (14)$$

where  $\chi_\delta = \partial p_{nH} / \partial |\delta|$ , and  $\chi_{\mathcal{D}_t} = \partial p_{nH} / \partial |\mathcal{D}_t|$ . When  $|\mathcal{D}_t| \sim |\delta| \ll 1$ , a small change of  $\lambda$  can lead to a significant change of  $|\mathcal{D}_t|$  and  $|\delta|$  on the same order of magnitudes of themselves, thereby giving rise to an apparent

change of  $p_{\text{nH}}(t, \lambda)$ . This feature thus indicates an extreme sensitivity of  $p_{\text{nH}}(t, \lambda)$  to  $\lambda$ .

As a comparison, we also consider the standard Hermitian scenario where  $H = \lambda V = \lambda \sigma_x$ . Accordingly, the probability of the system in state  $|0\rangle$  can be expressed as

$$p_{\text{H}}(t, \lambda) = \frac{1}{2} (1 + \cos 2\lambda t), \quad (15)$$

from which one immediately obtains the associated susceptibility as  $\chi_{\text{H}}(\lambda) = |\partial p_{\text{H}}(t, \lambda) / \partial \lambda| = |\sin(2\lambda t)|$ .

In an explicit sensing protocol, the measurement precision of  $\lambda$  in the language of error-propagating can be quantified through

$$\delta\lambda = \frac{\sigma}{\chi(\lambda)}, \quad (16)$$

where  $\sigma$  characterizes the measurement error of the probability in state  $|0\rangle$ , and  $\chi(\lambda)$  is chosen as  $\chi_{\text{nH}}(\lambda)$  or  $\chi_{\text{H}}(\lambda)$  depending on the sensing scheme that is exploited. In actual experiments, different categories of noise can contribute to  $\sigma$ . For clarity, we decompose  $\sigma$  into two components by considering its scaling relation with the measurement repetitions (denoted by  $N$ )

$$\sigma^2 = \sigma_{\text{CLT}}^2 + \sigma_{\text{nCLT}}^2, \quad (17)$$

where  $\sigma_{\text{CLT}} = \Theta(1/\sqrt{N})$  captures statistical noise that follows the central limit theorem (CLT), while  $\sigma_{\text{nCLT}}$  represents technical noises that cannot be efficiently suppressed by averaging through repetitive experiments. Here, the symbol  $\Theta(x)$  indicate an asymptotic scaling identical to  $x$  for large  $x$ . From Fig. 1, it can be seen that for small values of  $\delta$ ,

$$\mathcal{A} = \frac{\chi_{\text{nH}}(\lambda)}{\chi_{\text{H}}(\lambda)} \gg 1. \quad (18)$$

However, this does not simply implies that the non-Hermitian sensing scheme outperforms the Hermitian counterpart. This is due to that the success probability of implementing a non-Hermitian dynamics via dilation protocols into enlarged Hermitian systems is also very small for  $|\delta| \ll 1$ . Consequently, the number of available measurement trials for the non-Hermitian sensing would be much smaller than the Hermitian case under an identical number of total repetitive measurements  $N$ , i.e.  $N_{\text{nH}} \ll N_{\text{H}} = N$ .

Firstly, we consider the simple case where  $\sigma_{\text{nCLT}} = 0$ . In principle, one can achieve a success probability such that  $N_{\text{nH}} = \Theta(N/\mathcal{A}^2)$  [41]. As a result, the precision achieved by the non-Hermitian sensing scheme is comparable to the Hermitian counterpart,

$$\delta\lambda_{\text{nH}} = \frac{\sigma_{\text{CLT}}}{\chi_{\text{nH}}(\lambda)} \sim \frac{1/\sqrt{N/\mathcal{A}^2}}{\mathcal{A}\chi_{\text{H}}(\lambda)} \sim \frac{1/\sqrt{N}}{\chi_{\text{H}}(\lambda)} \sim \delta\lambda_{\text{H}}. \quad (19)$$

This result is consistent with the conclusion derived from the perspective of quantum Fisher information of the full

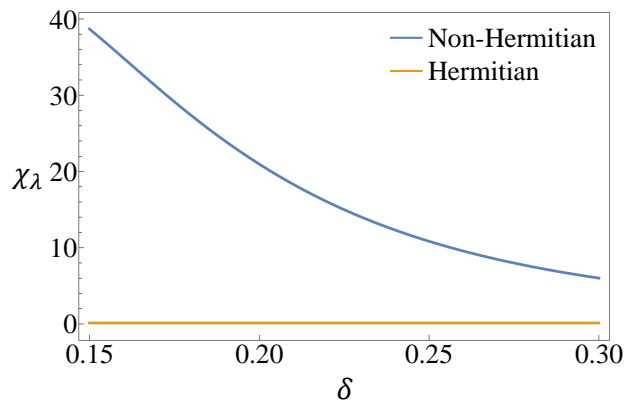


FIG. 1. **Relationship of the susceptibility  $\chi_\lambda$  with the control parameter  $\delta$ .** When  $|\mathcal{D}_t| \sim |\delta| \ll 1$ , the non-Hermitian system exhibits a sharply divergent response as  $|\delta| \rightarrow 0$ , which is much more prominent than the corresponding Hermitian evolution.

quantum system [41, 64]. Surprisingly, albeit the small success probability, the particular subensemble of the total measurements that yields the desired non-Hermitian dynamics is sufficient to achieve a precision of the same order as the full system. This feature indeed endows the non-Hermitian strategy a peculiar capability of suppressing technical noises.

Next, we focus on the realistic case that  $\sigma_{\text{nCLT}} \neq 0$ . Suppose that  $\sigma_{\text{nCLT}} = \Theta(N^{-\alpha})$  with  $\alpha < 1/2$ , which would be much larger than  $\sigma_{\text{CLT}} = \Theta(N^{-1/2})$  in the large- $N$  limit. Similarly, one can derive that

$$\delta\lambda_{\text{nH}} = \Theta\left(\frac{(N/\mathcal{A}^2)^{-\alpha}}{\chi_{\text{nH}}(\lambda)}\right) = \Theta(\mathcal{A}^{2\alpha-1}\delta\lambda_{\text{H}}). \quad (20)$$

This result clearly uncovers the significant advantage of non-Hermitian sensing in the large- $N$  limit to reduce experimental technical noises that can not be efficiently eliminated by repetitive measurements.

### III. TECHNICAL NOISE MODELS

In this section, we delineate the specific technical noise sources that contribute to the term,  $\sigma_{\text{nCLT}}$  in Eq. (17) that does not follow the central limit theorem. We focus on ubiquitous experimental constraints, including biased readout errors, background detection noise, systematic parameter offsets, and detector saturation. By analyzing these explicit noise models, we establish the fundamental conditions under which non-Hermitian sensing architectures provide a decisive advantage over conventional Hermitian protocols.

### A. Biased readout error

In state-of-the-art quantum sensing platforms, ranging from superconducting circuits to nitrogen-vacancy (NV) centers, readout fidelity remains a primary bottleneck for achievable sensitivity. Beyond fundamental quantum projection noise, the physical process of state measurement often introduces a systematic bias that persists regardless of the number of measurement repetitions  $N$ . This non-reducible error arises from inherent physical asymmetries during the readout window, which shift the observed signal away from its true value.

Consider a non-Hermitian qubit sensor following the signal interrogation stage. We perform  $N$  repeated measurements with outcomes  $N_0$  and  $N_1$  corresponding to states  $|0\rangle$  and  $|1\rangle$ , respectively. In an ideal scenario, the estimated probability,

$$p_0 = \frac{N_0}{N_0 + N_1}, \quad (21)$$

converges to the theoretical value predicted by Eq. (13) in the large- $N$  limit. In practice, however, hardware-specific imperfections and fixed experimental offsets during the readout pulse distort this distribution. This bias is typically rooted in the competition between the measurement timescale and the internal relaxation dynamics of the qubit.

In superconducting transmons or trapped ions, for instance, longitudinal relaxation ( $T_1$ ) during the dispersive readout pulse causes the excited state  $|1\rangle$  (often the “bright” state) to decay into the ground state  $|0\rangle$  (the “dark” state). Conversely, the upward transition  $|0\rangle \rightarrow |1\rangle$  is thermally suppressed at millikelvin temperatures. This results in an asymmetric error hierarchy where the “dark” error rate ( $\kappa_1$ , misidentifying  $|1\rangle$  as  $|0\rangle$ ) significantly outweighs the “bright” error rate ( $\kappa_0$ , misidentifying  $|0\rangle$  as  $|1\rangle$ ), systemically shifting the population toward the ground state.

For NV centers in diamond, the manifestation of this bias is reversed but follows a similar physical logic. Here, the  $m_s = 0$  state ( $|0\rangle$ ) serves as the “bright” state due to its high cycling fluorescence rate, while the  $m_s = \pm 1$  state ( $|1\rangle$ ) are “dark” due to non-radiative inter-system crossing. Biased readout errors emerge because the dark state can relax back into the bright state under continuous optical excitation, coupled with fixed offsets in the threshold settings of the photon counter. Furthermore, since photon emission follows a Poisson distribution with limited collection efficiency, the overlap between the high-count  $|0\rangle$  tail and the low-count  $|1\rangle$  tail is inherently asymmetric.

In both physical implementations, these state-dependent overlaps and transitions yield an observed probability:

$$p = p_0(1 - \kappa_0) + (1 - p_0)\kappa_1, \quad (22)$$

where  $\kappa_0$  and  $\kappa_1$  are misidentification rates of state  $|0\rangle$

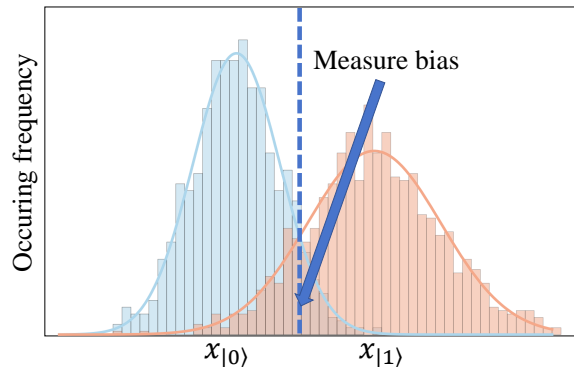


**FIG. 2. Statistics of quantum measurement outcomes and biased readout error.** Histograms of detected photon counts or the qubit prepared in the  $|0\rangle$  (blue) and  $|1\rangle$  (orange) states. In the presence of quantum projection noise and classical readout noise, the outcomes follow broadened Poissonian (or Gaussian) distributions centered at  $x_{|0\rangle}$  and  $x_{|1\rangle}$ . The finite overlap between the two distributions leads to misassignment errors, characterized by the probabilities  $\kappa_0$  and  $\kappa_1$ . Crucially, physical asymmetries—such as  $T_1$  relaxation in superconducting qubits or state-dependent decay in NV centers—result in an unequal overlap, where the “dark” error rate typically outweighs the “bright” error rate. This asymmetry induces a persistent measurement bias that imposes a systematic limit on sensing fidelity, which can be mitigated through the amplified response of non-Hermitian dynamics.

or  $|1\rangle$ , respectively. The resulting persistent offset,

$$\text{Bias}(p) = \kappa_1 - (\kappa_0 + \kappa_1)p_0 \quad (23)$$

imposes a systematic ceiling on precision that cannot be resolved by statistical averaging. This systematic offset is particularly detrimental in conventional Hermitian sensing protocols, such as Ramsey-type interferometry, where the optimal operating point is typically chosen at  $p_0 = 1/2$ , to maximize the linear response. At this point, any disparity between  $\kappa_0$  and  $\kappa_1$  introduces an intrinsic bias,  $\text{Bias}(p) = (\kappa_1 - \kappa_0)/2$ , which misaligns the sensor and compromises the accuracy of parameter estimation. In this regime, the utility of non-Hermitian dynamics becomes evident: by significantly amplifying the response function  $\chi_{\text{nH}}(\lambda)$ , the sensor can boost the signal magnitude far above this hardware-inherent bias. This amplification effectively “shields” the measurement from the deleterious effects of asymmetric readout noise, restoring high-fidelity sensing even in the presence of heavily overlapped or intrinsically biased distributions.

### B. Correlated background detection noise

Beyond state-assignment errors, quantum sensors are frequently subjected to background detection noise that exhibits significant temporal or spatial correlations. Unlike stochastic fluctuations that vanish in the large- $N$

limit, such correlated noise introduces a fundamental precision floor that cannot be bypassed by simple repetitive averaging. We consider a general scenario where the total measured signal is  $X_j = x_j + \xi_j$ , comprising the intrinsic qubit response  $x_j$  and the background detection noise  $\xi_j$ . To model the underlying statistics, we assume that  $x_j$  follows a mixture of two Gaussian distributions:

$$x_j \sim p_0 \mathcal{N}(x_{|0\rangle}, \sigma^2) + (1 - p_0) \mathcal{N}(x_{|1\rangle}, \sigma^2), \quad (24)$$

with the corresponding mean and variance given by

$$\begin{aligned} \mathbb{E}[x_j] &= p_0 x_{|0\rangle} + (1 - p_0) x_{|1\rangle}, \\ \text{Var}[x_j] &= p_0(1 - p_0)x^2 + \sigma^2, \end{aligned} \quad (25)$$

where  $x = x_{|0\rangle} - x_{|1\rangle}$  defines the signal contrast.

In this correlated regime, the background noise  $\{\xi_j\}_{j=1}^N$  is modeled as a multivariate Gaussian distribution with zero mean and a non-diagonal covariance matrix  $\mathbf{C}$ :

$$P(\xi) = \frac{1}{\sqrt{(2\pi)^N \det \mathbf{C}}} \exp\left[-\frac{\xi^T \mathbf{C}^{-1} \xi}{2}\right]. \quad (26)$$

To evaluate the impact of these correlations, we utilize the probability estimator

$$\hat{p} = \frac{1}{Nx} \sum_j (X_j - x_{|1\rangle}). \quad (27)$$

By assuming the expectation value  $\mathbb{E}[X_j] = p_0 x_{|0\rangle} + (1 - p_0) x_{|1\rangle}$  (temporarily setting aside biased readout errors for clarity), we find that  $\mathbb{E}[\hat{p}] = p_0$ , identifying  $\hat{p}$  as an unbiased estimator of the population in state  $|0\rangle$ .

The performance of the sensor is dictated by the variance of this estimator, which reveals the scaling laws of the noise:

$$\begin{aligned} \text{Var}[\hat{p}] &= \frac{1}{N^2 x^2} \sum_{ij} \mathbb{E}[(X_i - \mathbb{E}[X_i])(X_j - \mathbb{E}[X_j])] \\ &= \frac{1}{N^2 x^2} \sum_i \text{Var}[x_i] + \frac{1}{N^2 x^2} \sum_{ij} \mathbb{E}[\xi_i \xi_j] \\ &= \frac{p_0(1 - p_0)}{N} + \frac{\sigma^2}{Nx^2} + \frac{1}{N^2 x^2} \sum_{ij} \mathbb{E}[\xi_i \xi_j]. \end{aligned} \quad (28)$$

In accordance with the noise decomposition in Eq. (17), the terms scaling as  $1/N$  constitute the standard CLT contribution,

$$\sigma_{\text{CLT}}^2 = \frac{p_0(1 - p_0)}{N} + \frac{\sigma^2}{Nx^2} \quad (29)$$

originating from quantum projection noise and photon shot noise, respectively. However, the influence of correlated background detection noise is quantified by the non-standard term:

$$\sigma_{\text{nCLT}}^2 = \frac{1}{N^2 x^2} \sum_{ij} \mathbb{E}[\xi_i \xi_j] = \frac{1}{N^2 x^2} \sum_{ij} \mathbf{C}_{ij}. \quad (30)$$

For many physical detection systems, the noise satisfies translational invariance in the time or spatial domain, such that the correlation depends only on the interval between measurements, i.e.  $\mathbf{C}_{ij} = \mathcal{C}(|i - j|)$ . Typically, these correlations decay as the separation  $|i - j|$  increases, following a characteristic decay length or time constant. If the correlations decay sufficiently fast (e.g., exponentially or as a power law with a large exponent), the sum  $\sum_j \mathcal{C}(|i - j|)$  converges to a constant value independent of  $N$ . In this short-range correlated limit, the total sum  $\sum_{ij} \mathbf{C}_{ij}$  scales linearly with  $N$ , and the noise behaves similarly to white noise, effectively vanishing as  $1/N$  in the estimator variance. However, for systems exhibiting long-range correlations or  $1/f$ -type noise, the sum  $\sum_{ij} \mathbf{C}_{ij}$  scales as  $N^\beta$  with  $\beta \in (1, 2]$ , which further leads to that  $\alpha = 1 - \beta/2$  in Eq. (20) and indicates the emergence of quantum advantage offered by non-Hermitian sensing schemes. In the extreme case of perfect correlation (where  $\mathbf{C}_{ij} = \sigma_\xi^2$  for all  $i, j$ ; that is  $\beta \rightarrow 2$ ), the background noise constitutes a completely non-reducible noise floor, which cannot be mitigated by increasing measurement repetitions  $N$  and imposes a fundamental ceiling on the sensitivity of conventional protocols. Non-Hermitian sensing architectures overcome this by amplifying the response function  $\chi_{\text{nH}}(\lambda)$ , effectively boosting the signal relative to this persistent noise floor and restoring metrological scaling advantages in the presence of technical correlations.

For clarity, below we explicitly investigate the scaling behavior of  $\sum_{ij} \mathbf{C}_{ij}$  versus  $N$ . We define that

$$S_N = \sum_{i=1}^N \sum_{j=1}^N \mathbf{C}_{ij}. \quad (31)$$

Since the number of pairs with separation  $d = |i - j|$  is  $2(N - d)$  for  $d \geq 1$ , one obtains

$$\begin{aligned} S_N &= N\mathcal{C}(0) + 2 \sum_{d=1}^{N-1} (N - d)\mathcal{C}(d) \\ &= N\mathcal{C}(0) + 2N \sum_{d=1}^{N-1} \mathcal{C}(d) - 2 \sum_{d=1}^{N-1} d\mathcal{C}(d). \end{aligned} \quad (32)$$

Suppose that the correlation function decays algebraically as

$$\mathcal{C}(d) \sim c d^{-\gamma}, \quad \gamma > 0,$$

the asymptotic behavior of  $S_N$  in the larger  $N$  limit is determined by  $\sum_{d=1}^{N-1} d^{-\gamma}$  and  $\sum_{d=1}^{N-1} d^{1-\gamma}$ . For  $0 < \gamma < 1$ , both contributions scale as  $N^{2-\gamma}$ , yielding that

$$S_N \sim N^{2-\gamma}.$$

For the marginal case  $\gamma = 1$ , one obtains a logarithmic correction,

$$S_N \sim N \log N.$$

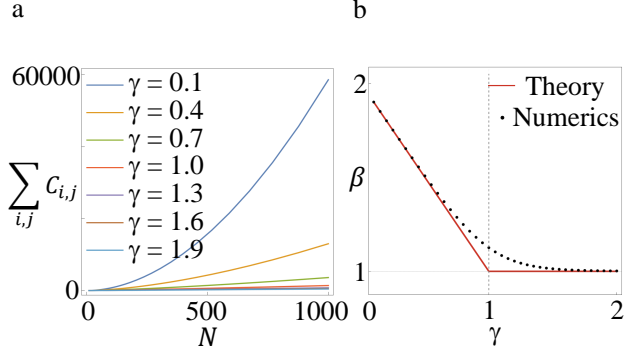


FIG. 3. **Scaling behavior of correlated background detection noise.** We consider power-law correlations in the background noise, with the correlation function defined as  $C(|i-j|) \sim |i-j|^{-\gamma}$ , where the exponent  $\gamma$  governs the spatial decay rate. (a) Total noise correlation  $\sum_{i,j} C_{i,j}$  as a function of the number of measurements  $N$  for different values of  $\gamma$ . In the short-range regime ( $\gamma > 1$ ), the total sum exhibits standard linear scaling  $\sum_{i,j} C_{i,j} \propto N$ . In contrast, for long-range correlations ( $\gamma < 1$ ), the sum diverges super-extensively as  $\sum_{i,j} C_{i,j} \propto N^\beta$  with  $\beta = 2 - \gamma$ . (b) The extracted scaling exponent  $\beta$  as a function of the correlation exponent  $\gamma$ . A clear crossover occurs at the critical value  $\gamma = 1$ : for  $\gamma > 1$ , the noise is effectively uncorrelated with  $\beta \approx 1$ , whereas for  $\gamma < 1$ , the scaling is dominated by long-range dependencies, following the predicted relation  $\beta = 2 - \gamma$ . This superlinear growth of background noise directly impacts the metrological gain of non-Hermitian sensors in practical environments.

By contrast, for  $\gamma > 1$ ,  $S_N$  is dominated by the first two terms and scales as

$$S_N \sim N.$$

Hence, for algebraically decaying correlations, the scaling exponent  $\beta$  defined through  $S_N \sim N^\beta$  is given by

$$\beta = \begin{cases} 2 - \gamma, & 0 < \gamma < 1, \\ 1, & \gamma > 1. \end{cases}$$

This result explicitly shows that short-range correlated background noise ( $\gamma > 1$ ) remains extensive and lead to the usual  $1/N$  influence on the estimator variance, whereas long-range correlations ( $0 < \gamma < 1$ ) produce super-extensive noise accumulation,  $S_N \sim N^\beta$  with  $1 < \beta < 2$ . More specifically, using that  $\alpha = 1 - \beta/2$ , one obtains that

$$\alpha = \begin{cases} \gamma/2, & 0 < \gamma < 1, \\ 1/2, & \gamma > 1. \end{cases}$$

This result, together with the principle in Eq. (20), clearly identifies the fact that non-Hermitian sensing can lead to significant advantage over conventional Hermitian protocols for long-range correlated background detection noise.

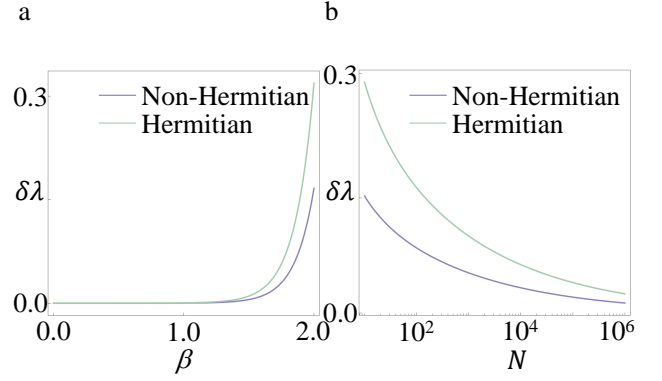


FIG. 4. **Measurement precision under correlated background detection.** We compare the estimation precision of the parameter  $\lambda$  for Hermitian and non-Hermitian sensors in the presence of background noise with long-range correlations characterized by the exponent  $\beta$ . Parameters of the non-Hermitian sensing are set to  $t = \pi/2\mathcal{E}$  with  $a = 1$ ,  $\delta = 0.3$ ,  $\mathcal{E} = 0.5$ ,  $\lambda = 0.01$ . (a) Precision as a function of the correlation coefficient  $\beta$  for a fixed number of measurements  $N = 1000$ . The non-Hermitian protocol demonstrates a significant enhancement over the Hermitian counterpart as  $\beta$  approaches 2, a regime where long-range correlations severely degrade standard sensing performance. (b) Scaling of the precision with the measurement repetitions  $N$  for highly correlated noise ( $\beta = 1.8$ ). Notably, the non-Hermitian sensor displays an apparent advantage in measurement precision over the Hermitian counterpart.

### C. Systematic parameter offsets

Beyond the stochastic detection noise discussed above, the achievable precision is often fundamentally limited by our incomplete knowledge of the sensing apparatus itself. This epistemic uncertainty manifests as systematic parameter offsets that, unlike statistical fluctuations, cannot be suppressed simply by increasing the measurement repetitions  $N$ .

To formalize this, consider a scenario where the measurement outcome  $\hat{p}$  depends not only on the target parameter  $\lambda$ , but also on a set of nuisance parameters governing the experimental setting. We categorize these into two distinct classes: fluctuating parameters  $\hat{\kappa}$ , and fixed unknown parameters  $\zeta$ . The fluctuating term  $\hat{\kappa}$  varies stochastically between individual measurements (e.g., shot-to-shot laser intensity drift). For the  $j$ -th measurement, its value  $\hat{\kappa}_j$  follows a distribution with mean  $\bar{\kappa}$  and variance  $(\Delta\kappa)^2$ . In contrast, the parameter  $\zeta$  represents a systematic calibration offset (e.g., a fixed misalignment or cavity detuning) that remains constant,  $\zeta_r$ , across the entire ensemble of  $N$  repetitions. However, the observer lacks access to the exact value  $\zeta_r$ , relying instead on a prior estimation  $\zeta_p$  characterized by a uncertainty  $(\Delta\zeta)^2$ .

To reconstruct the true value of the target parameter, denoted as  $\lambda_r$ , we define the signal expectation value

analytically as

$$p(\lambda, \zeta, \hat{\kappa}) \equiv \mathbb{E}[\hat{p}] = \int \hat{p} \cdot P(\hat{p} | \lambda, \zeta, \hat{\kappa}) d\hat{p}, \quad (33)$$

where  $P(\hat{p} | \lambda, \zeta, \hat{\kappa})$  represents the probability distribution of  $\hat{p}$  depending on  $\{\lambda, \zeta, \hat{\kappa}\}$ . Accordingly, we find that

$$p(\lambda_r, \zeta_r, \hat{\kappa}_j) \equiv \mathbb{E}[\hat{p}_j] = \int \hat{p}_j \cdot P(\hat{p}_j | \lambda_r, \zeta_r, \hat{\kappa}_j) d\hat{p}_j, \quad (34)$$

where  $\hat{p}_j$  is the  $j$ -th measurement outcome sampled from the physical distribution  $P(\hat{p}_j | \lambda_r, \zeta_r, \hat{\kappa}_j)$ . The observer constructs an estimator  $\hat{\lambda}$  by equating the theoretical expectation to the empirical mean:

$$p(\hat{\lambda}, \zeta_p, \bar{\kappa}) = \frac{1}{N} \sum_{j=1}^N \hat{p}_j, \quad (35)$$

By linearizing the signal function around  $\{\lambda_r, \zeta_r, \bar{\kappa}\}$ , i.e. subtracting  $p(\hat{\lambda}, \zeta_p, \bar{\kappa})$  and  $\sum_{j=1}^N p(\lambda_r, \zeta_r, \hat{\kappa}_j)/N$ , the deviation of the estimator can be expressed as

$$\begin{aligned} & \frac{1}{N} \sum_{i=1}^N (\hat{p}_i - \mathbb{E}[\hat{p}_i]) \\ &= \frac{\partial p}{\partial \lambda} (\hat{\lambda} - \lambda_r) + \frac{\partial p}{\partial \zeta} (\zeta_p - \zeta_r) - \frac{1}{N} \sum_{i=1}^N \frac{\partial p}{\partial \kappa} (\kappa_i - \bar{\kappa}). \end{aligned} \quad (36)$$

Based on this formula, the measurement precision of  $\lambda$  can be quantified as

$$\begin{aligned} (\delta\lambda)^2 &= \mathbb{E}[(\hat{\lambda} - \lambda_r)^2] \\ &= \frac{1}{|\partial_\lambda p|^2} \left[ \frac{(\Delta p)^2 + |\partial_\kappa p|^2 (\Delta\kappa)^2}{N} + |\partial_\zeta p|^2 (\Delta\zeta)^2 \right]. \end{aligned} \quad (37)$$

Here, the three terms correspond to readout noise (i.e.  $(\Delta p)^2 = \sum_{i=1}^N \mathbb{E}[(\hat{p}_i - \mathbb{E}[\hat{p}_j])^2]/N$ , parameter fluctuations, and systematic calibration error, respectively.

This result highlights a critical hierarchy in noise scaling. The first term in the brackets scales as  $1/N$ , encompassing both readout noise and reproducible parameter fluctuations; these are efficiently reducible via averaging. By invoking the noise decomposition formula in Eq. (17)], the last term yields that

$$\sigma_{\text{nCLT}}^2 = |\partial_\zeta p|^2 (\Delta\zeta)^2 \quad (38)$$

This term represents a non-reducible systematic floor arising from the consistent error in the experimental setting. Crucially, while Hermitian averaging strategies can only minimize the first term, non-Hermitian sensing offers a unique advantage against the second. By engineering the system to operate at  $\chi_{\text{nH}} \gg 1$ , one can effectively suppress the impact of the fixed systematic floor  $\sigma_{\text{nCLT}}^2$ , enabling precision regimes inaccessible to conventional sensors bounded by calibration uncertainties.

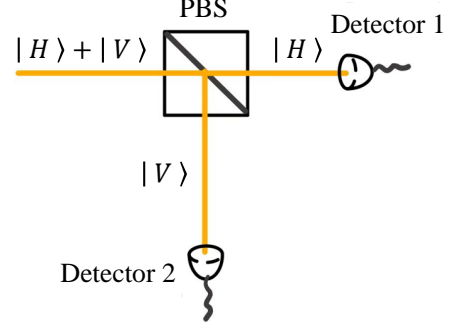


FIG. 5. Schematic diagram of the photodetector. The horizontal and vertical polarization states ( $|H\rangle, |V\rangle$ ) of a photon are commonly used to encode two orthogonal quantum states, and their measurement can be realized using a polarization beam splitter (PBS). Detector 1 and detector 2 are photodetectors, which measure the two different polarization directions of photons obtained through the beam splitter. The number of photons measured by the two detectors follows a normal distribution.

#### D. Detector saturation noise

Detector saturation is a common limitation in optical experiments (see Fig. 5). A detector, such as a camera, converts the number of photons incident on each pixel into an electrical signal. Owing to the intrinsic limit on the number of photons that a detector can accurately measure, the detector output inevitably approaches a constant value as the incident photon number increases. Just Let  $k_{\text{max}}$  denote the maximum output count of a pixel, and  $N_{\text{sat}}$  represent the characteristic scale of the saturation photon number. When the number of photons reaching the pixel  $N \geq N_{\text{sat}}$ , the pixel output exhibits a pronounced saturation behavior, analogous to a compression or flattening effect [65].

For photons in a coherent state, the probability distribution of the number of photons incident on each pixel such as pixel  $j$  follows a Poisson distribution:

$$P(N_j) = \frac{\bar{n}_j^{N_j} e^{-\bar{n}_j}}{N_j!} \quad (39)$$

where the mean photon number for a given pixel is given by the integral of the wavefunction over the pixel area multiplied by the total photon number  $n$ , as  $\bar{n}_j = n \int_j |\psi(x)|^2 dx$ .

Then each pixel converts the incident photons into an electrical signal. Owing to the presence of output noise at the pixel level, the electrical signal  $k_j$  of pixel  $j$  could be described by a Gaussian distribution  $k_j \sim \mathcal{N}(\mu_j, \sigma^2)$ , expressed in a discrete, normalized form:

$$P(k_j | N_j) = \frac{e^{-(k_j - \mu_j)^2 / 2\sigma^2}}{\sum_{k_j'} e^{-(k_j' - \mu_j)^2 / 2\sigma^2}} \quad (40)$$

Here,  $\mu_j$  is the key parameter governing the onset of saturation, whereas  $\sigma$  arises from detector pixel noise—e.g., signal-spread uncertainty induced by shot noise. In the absence of saturation effects, it is evident that  $\mu_j \propto N_j$ . However, owing to the presence of saturation effects, the mean of the Gaussian distribution describing the output of each pixel is reduced relative to its ideal value. By choosing  $\mu_j = k_{\max}(1 - e^{-N_j/N_{\text{sat}}})$ , it is easy to observe that  $k_j \approx k_{\max}N_j/N_{\text{sat}}$  for  $N \ll N_{\text{sat}}$  but  $k_j$  saturates to  $k_{\max}$  at  $N_{\text{sat}}$  as  $N$  increases to approach or exceed  $N_{\text{sat}}$ . So, the probability of obtaining the pixel output  $k_j$  on pixel  $j$  can be written using the total probability theorem as:

$$P(k_j) = \sum_{N_j} P(k_j | N_j) \cdot P(N_j) \quad (41)$$

By summing the products of the probabilities of obtaining different values of  $N_j$  and the corresponding  $P(k_j | N_j)$  at each  $N_j$ , the result can be obtained. On this basis, it is straightforward to write down  $\mathbb{E}[k_j]$  and  $\mathbb{E}[k_j^2]$ .

$$\begin{aligned} \mathbb{E}[k_j] &= \sum_{k_j} k_j \sum_{N_j} P(k_j | N_j) \cdot P(N_j) \\ &= \sum_{N_j} P(N_j) \sum_{k_j} k_j P(k_j | N_j) = \sum_{N_j} P(N_j) \mathbb{E}[k | N_j] \\ \mathbb{E}[k_j^2] &= \sum_{k_j} k_j^2 \sum_{N_j} P(k_j | N_j) \cdot P(N_j) \\ &= \sum_{N_j} P(N_j) \sum_{k_j} k_j^2 P(k_j | N_j) = \sum_{N_j} P(N_j) \mathbb{E}[k^2 | N_j] \end{aligned} \quad (42)$$

Utilize  $\mathbb{E}[k^2 | N_j] = \text{Var}(k | N_j) + (\mathbb{E}[k | N_j])^2$ , applying the same procedure to  $\text{Var}(k_j)$ , we could obtain the final measurement variance of single pixel on detector:

$$\begin{aligned} \text{Var}(k_j) &= \sum_{N_j} P(N_j) \text{Var}(k_j | N_j) + \sum_{N_j} P(N_j) (\mathbb{E}[k_j | N_j])^2 \\ &\quad - \left( \sum_{N_j} P(N_j) \mathbb{E}[k_j | N_j] \right)^2 \\ &= \mathbb{E}_N[\text{Var}(k_j | N_j)] + \text{Var}_N(\mathbb{E}[k_j | N_j]) \end{aligned} \quad (43)$$

Although  $P(k_j | N_j)$  is defined in a discrete form, by approximating it as a continuous variable, it is easy to obtain  $\mathbb{E}[k_j | N_j] = \mu_j(N_j)$  and  $\text{Var}(k_j | N_j) = \sigma^2$ . So the  $\text{Var}(k_j)$  could then reduce to a very compact form.

$$\text{Var}(k_j) = \sigma^2 + \text{Var}_N[\mu_j(N_j)] \quad (44)$$

Next, we only need to calculate  $\text{Var}_N[\mu_j(N_j)]$ , which can be obtained directly from  $\mu_j = k_{\max}(1 - e^{-N_j/N_{\text{sat}}})$ .

$$\begin{aligned} \text{Var}_N[\mu_j(N_j)] &= k_{\max}^2 \cdot \text{Var}_N(e^{-N_j/N_{\text{sat}}}) \\ &= k_{\max}^2 \cdot (\mathbb{E}[e^{-2N_j/N_{\text{sat}}}] - (\mathbb{E}[e^{-N_j/N_{\text{sat}}}]^2)) \end{aligned} \quad (45)$$

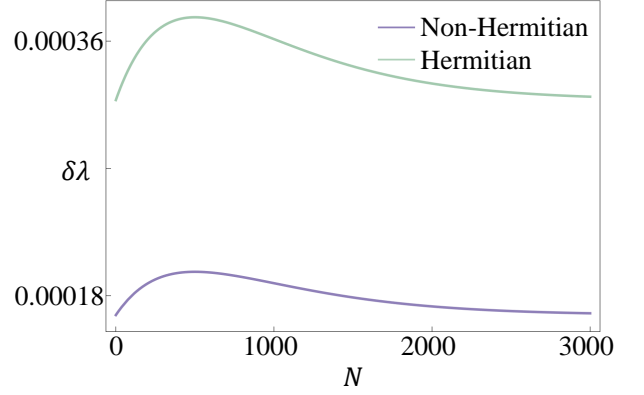


FIG. 6. **Precision of  $\lambda$  of Hermitian and non-Hermitian sensors as a function of  $N$  in the presence of detector saturation noise.** The detector saturation threshold is set to  $N_{\text{sat}} = 1 \times 10^3$ . For fixed evolution time  $t = \pi/2\mathcal{E}$  with  $a = 1$ ,  $\delta = 0.3$  and  $\lambda = 0.01$ , non-Hermitian sensing outperforms Hermitian sensing under the influence of saturation effects. When measurement repetitions  $N$  is much less than  $N_{\text{sat}}$ , the sensitivity would increase. And when  $N$  is approaching to even exceed to the  $N_{\text{sat}}$ , sensitivity growth would stabilize and then decrease in the opposite direction.

among this  $\mathbb{E}[e^{-2N_j/N_{\text{sat}}}] = \sum_{N_j} P(N_j)e^{-2N_j/N_{\text{sat}}}$  and  $\mathbb{E}[e^{-N_j/N_{\text{sat}}}]$  has the same form. As mentioned earlier,  $P(N_j)$  follows a Poisson distribution. From the probability generating function of the Poisson distribution, one finds that for  $N \sim \text{Poisson}(\lambda)$ ,  $\mathbb{E}[a^N] = e^{\lambda(a-1)}$  can be obtained. Therefore,

$$\begin{aligned} \text{Var}(k_j) &= \sigma^2 + k_{\max}^2 \cdot \{ \exp[\bar{n}_j(e^{-2/N_{\text{sat}}} - 1)] \\ &\quad - \exp[2\bar{n}_j(e^{-1/N_{\text{sat}}} - 1)] \} \end{aligned} \quad (46)$$

The first term of the variance originates from the intrinsic noise of the detector and can be reduced by increasing the number of repeated measurements. The second term arises from detector saturation and cannot be suppressed by repetition. This behavior is consistent with physical intuition: when the measured photon number  $N_j$  approaches the saturation threshold  $N_{\text{sat}}$ , photon numbers incident on a pixel that differ substantially can be mapped by the saturation effect onto much closer measured signals  $k_j$ . Under the influence of detector noise, ideal photon numbers that would otherwise be uncorrelated acquire a higher probability of being mapped to the same measured signal. This effectively establishes correlations between different photon-number outcomes, leading to a variance term that cannot be reduced through repeated measurements. It is precisely this term that reflects the advantage of non-Hermitian quantum sensing.

#### IV. INFORMATION-THEORETIC ANALYSIS

In this section, we rigorously quantify the metrological advantage of non-Hermitian protocols using the frame-

work of parameter estimation theory. Our analysis centers on two fundamental figures of merit: the quantum Fisher information (QFI),  $\mathcal{F}_\lambda$ , and the classical Fisher information (FI)  $F_\lambda$ . These quantities establish the ultimate precision limits for estimating an unknown parameter  $\lambda$  via the Cramér–Rao bound:

$$(\delta\lambda)^2 \geq \frac{1}{N\mathcal{F}_\lambda} \geq \frac{1}{N\mathcal{F}_\lambda}, \quad (47)$$

where  $N$  denotes the number of independent measurements. Therefore, a larger QFI or FI signifies a better achievable estimation uncertainty.

### A. Basic concepts

The QFI represents the maximum extractable information inherent in a quantum state,  $\rho_\lambda$ , independent of the specific measurement scheme. It is defined as

$$\mathcal{F}_\lambda = \text{Tr} [\rho_\lambda L_\lambda^2], \quad (48)$$

where the symmetric logarithmic derivative  $L_\lambda$  is the Hermitian operator satisfying the Lyapunov equation

$$\frac{\partial \rho_\lambda}{\partial \lambda} = \frac{1}{2} (\rho_\lambda L_\lambda + L_\lambda \rho_\lambda). \quad (49)$$

For pure-state metrology, i.e.  $\rho_\lambda = |\psi_\lambda\rangle\langle\psi_\lambda|$ , the QFI (by solving the above two equations) can be expressed in the following form,

$$\mathcal{F}_\lambda = 4 \left( \langle \partial_\lambda \psi_\lambda | \partial_\lambda \psi_\lambda \rangle - |\langle \partial_\lambda \psi_\lambda | \psi_\lambda \rangle|^2 \right). \quad (50)$$

While QFI sets the theoretical ceiling, the classical FI,  $F_\lambda$ , quantifies the information actually retrieved by a specific measurement apparatus. Given a measurement outcome  $x$ , governed by the conditional probability distribution  $P(x|\lambda)$ , the FI is the variance of the score function:

$$F_\lambda = \int P(x|\lambda) \left[ \frac{\partial}{\partial \lambda} \ln P(x|\lambda) \right]^2 dx. \quad (51)$$

Physically,  $F_\lambda$  characterizes the sensitivity of the likelihood function  $P(x|\lambda)$  to infinitesimal changes in  $\lambda$ . A broader distribution implies lower FI, whereas sharp, rapidly shifting distributions yield high FI. In experimental contexts,  $F_\lambda$  serves as the practical benchmark, capturing the interplay between the intrinsic quantum sensitivity and the inevitable broadening induced by readout noise and finite statistics.

### B. Physical constraints on QFI in non-Hermitian dilation

The purported sensitivity advantage of non-Hermitian systems often manifests as a divergence in the QFI calculated directly from the effective non-Hermitian state

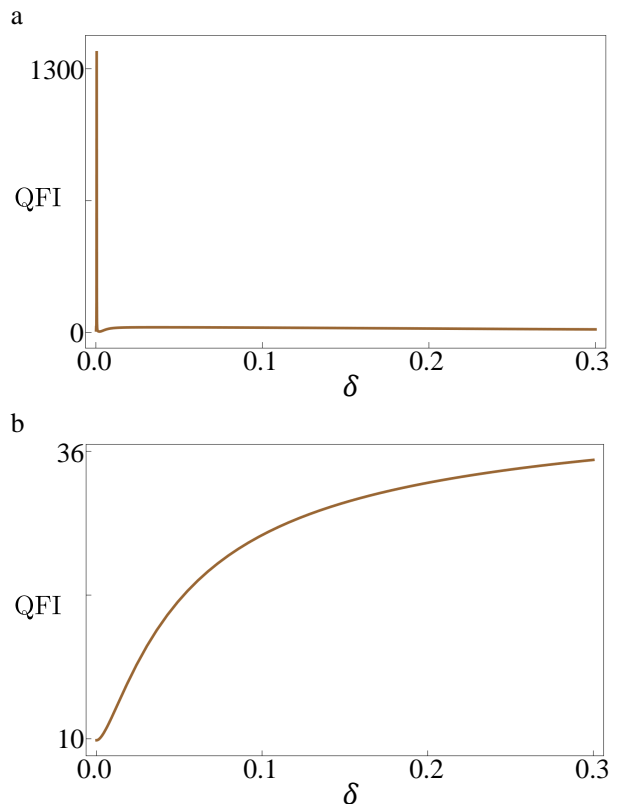


FIG. 7. **Quantum Fisher information (QFI) for non-Hermitian sensing as a function of  $\delta$ , without (a) and with (b) the successful probability of postselected non-Hermitian evolution.** Parameters: fixed evolution time  $t = \pi/2\mathcal{E}$ ,  $a = 1$  and  $\lambda = 0.01$ . Without accounting for the finite success probability, the QFI appears divergent in (a). Correctly including the success probability renders the QFI finite in (b), showing that non-Hermitian sensing does not yield an intrinsic QFI advantage in the absence of technical noise.

$|\psi(t)\rangle$  in Eq. (11). However, a rigorous metrological assessment requires accounting for the physical realization of such dynamics. Since any non-Hermitian Hamiltonian must be embedded into a larger, unitary Hermitian space to be experimentally implemented—a process known as Hermitian dilation—the resulting state evolution is inherently probabilistic.

Following the dilation framework for pseudo-Hermitian systems [49, 66], we consider an augmented Hermitian Hamiltonian  $H_{\text{tot}}$  acting on an extended Hilbert space,  $\mathcal{H}_{\text{sys}} \otimes \mathcal{H}_{\text{anc}}$ . A common construction utilizes:

$$H_{\text{tot}} = \Lambda \otimes I + \Gamma \otimes \sigma_z + \lambda \sigma_z \otimes I, \quad (52)$$

where  $\Lambda$  and  $\Gamma$  are Hermitian operators derived from the non-Hermitian target Hamiltonian and a metric-related operator  $M = \text{diag}[1, a/\delta^2]$ . Specifically,

$$\begin{aligned} \Gamma &= i(\mathcal{H}_{\text{sys}}U - U\mathcal{H}_{\text{sys}})M^{-1}, \\ \Lambda &= (\mathcal{H}_{\text{sys}} + U\mathcal{H}_{\text{sys}}U)M^{-1}. \end{aligned} \quad (53)$$

where  $U = \sqrt{M - I}$ . We remark that this dilated Hermitian system interacts with the unknown parameter  $\lambda$  in a standard linear form.

Starting from an initial state  $|\Psi(0)\rangle = [1/\sqrt{2}, -i/\sqrt{2}, 0, 0]^T$ , the global unitary evolution  $|\Psi(t)\rangle = e^{-iH_{\text{tot}}t}|\Psi(0)\rangle$  can be partitioned as:

$$|\Psi(t)\rangle = |\psi\rangle \otimes |-\rangle + |\zeta\rangle \otimes |+\rangle \quad (54)$$

where  $|\psi(t)\rangle$  corresponds to the state evolved under an effective non-Hermitian Hamiltonian, and  $P_s = \|(I \otimes |-\rangle\langle -|)\Psi(t)\|^2$  is the success probability of the post-selection measurement on the ancilla.

If the success probability is neglected, a "naive" calculation using  $|\psi(t)\rangle$  in Eq. (50) suggests a divergent QFI near if  $\delta \rightarrow 0$ , as shown in Fig. 7b. However, the operational QFI must be weighted by the probability of successfully projecting the system onto the non-Hermitian subspace. When this success probability  $P_s$  is properly accounted for, the divergent scaling vanishes, yielding the finite precision limits illustrated in Fig. 7a.

This result aligns with fundamental metrological bounds: since non-Hermitian dynamics are sub-processes within a larger unitary framework, the achievable information content cannot exceed the QFI of the underlying Hermitian system [41, 67]. Consequently, in the ideal, noiseless limit, non-Hermitian sensing offers no intrinsic QFI advantage over conventional Hermitian protocols. The genuine utility of non-Hermitian architectures must therefore be sought not in the reduction of statistical projection noise, but in their robustness against the technical and non-reducible noise floors prevalent in practical hardware.

### C. FI analysis in the presence technical noise

While the QFI provides a theoretical ceiling for sensing precision, its operational utility is often masked by the probabilistic nature of non-Hermitian implementations. To bridge the gap between abstract sensitivity and experimental reality, we turn to the FI,  $F_\lambda$ . Unlike the QFI, the FI directly characterizes the statistics of measurement outcomes, making it the natural framework for incorporating the non-reducible technical noises—readout bias, systematic offsets, and detector saturation—identified in Sec. III.

In realistic sensing scenarios, deriving closed-form expressions for the FI under a full noise-weighted density matrix is often intractable. Here, we adopt a data-driven approach by evaluating the FI through sufficient statistics derived from the outcome distributions. First, we determine the ideal probability of state  $|0\rangle$ , following non-Hermitian interrogation, as defined by Eq.(13). We then account for experimental imperfections by generating Monte Carlo samples of measurement outcomes for both Hermitian and non-Hermitian protocols, subjecting them to the noise models delineated previously. The

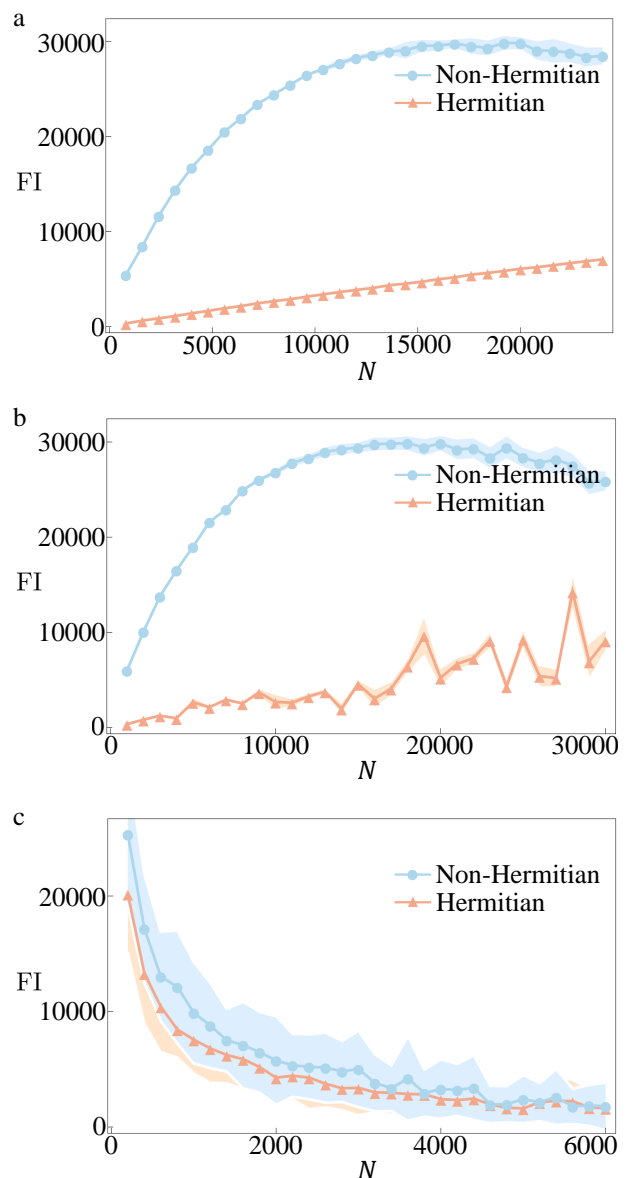


FIG. 8. **Classical Fisher information (FI) of non-Hermitian versus Hermitian sensing in the presence of technical noises.** By generating Monte Carlo samples with (a) correlated background detection noise, (b) systematic parameter offsets, and (c) detector saturation noise, use there data to calculate the corresponding FI of non-Hermitian and Hermitian protocols. Parameters setting:  $t = \pi/2\mathcal{E}$ ,  $a = 0.5$ ,  $\mathcal{E} = 1$ ,  $\delta = 0.2$ ,  $\lambda = 0.01$  and saturation threshold is  $N_{\text{sat}} = 1000$  in (c). In all cases, non-Hermitian sensing larger FI, demonstrating enhanced performance under the influence of these technical noises.

empirical FI is then numerically estimated via the finite-difference approximation.

In realistic experiments, the observable statistics are not directly governed by the ideal projection probability onto the  $|0\rangle$  state, denoted by  $S$ , but rather by an underlying physical parameter  $\lambda$  through the system re-

sponse function  $S(\lambda)$ . Consequently, the Fisher information must be defined with respect to the target parameter  $\lambda$ , instead of the effective probability  $S$ , as

$$F_\lambda = \mathbb{E} \left[ \left( \frac{\partial}{\partial \lambda} \ln p(\nu | \lambda) \right)^2 \right] = \int \frac{(\partial_\lambda p(\nu | \lambda))^2}{p(\nu | \lambda)} d\nu, \quad (55)$$

where  $p(\nu | \lambda)$  denotes the probability distribution of the experimentally accessible observable  $\nu$  in the presence of noise.

Due to the combined effects of various technical noise, an analytical expression for  $p(\nu | \lambda)$  is generally unavailable. We therefore estimate the Fisher information numerically using a Monte Carlo approach. For a fixed value of  $\lambda$ , the corresponding effective probability  $S(\lambda)$  is first determined from the system model. Based on this value, two stochastic count variables are generated according to Poisson statistics,  $n_0 \sim \text{Poisson}[S(\lambda)N_t]$  and  $n_1 \sim \text{Poisson}[(1 - S(\lambda))N_t]$ , where  $N_t$  denotes the total measurement resource. To model experimental imperfections, additive noise terms are further introduced, yielding the final observable in the form of a normalized ratio,

$$\nu = \frac{n_0 + \xi_0}{n_0 + n_1 + \xi_0 + \xi_1}, \quad (56)$$

with  $\xi_0$  and  $\xi_1$  drawn from prescribed noise distributions.

Repeating this procedure generates a sample ensemble of  $\nu$ , from which the probability distribution  $p(\nu | \lambda)$  is estimated via histogram binning with fixed bin boundaries. The resulting discrete probabilities are denoted by  $p_m(\lambda) \approx \text{P}(\nu \in \text{bin } m | \lambda)$ . Here, the index  $m$  labels the histogram bins used to discretize the continuous observable  $\nu$ , and  $p_m(\lambda)$  denotes the probability that  $\nu$  falls into the  $m$ -th bin. To approximate the derivative  $\partial_\lambda p_m(\lambda)$ , the same simulation is performed at a nearby parameter value  $\lambda + \Delta\lambda$  (equivalently through  $S(\lambda + \Delta\lambda)$ ), and a finite-difference scheme is employed,

$$\partial_\lambda p_m(\lambda) \approx \frac{p_m(\lambda + \Delta\lambda) - p_m(\lambda)}{\Delta\lambda}. \quad (57)$$

The Fisher information is then computed using the discrete form

$$F_\lambda \approx \sum_m \frac{[\partial_\lambda p_m(\lambda)]^2}{p_m(\lambda)}. \quad (58)$$

To quantify the statistical uncertainty arising from finite sampling, the above procedure is repeated multiple times for each  $N_t$ , and the mean and variance of the resulting Fisher information estimates are evaluated. This approach enables a systematic characterization of how the achievable information about  $\lambda$  depends on measurement resources and noise, while fully incorporating the nonlinear and stochastic nature of the experimental readout process.

The numerical results, presented in Fig. 8, reveal a consistent and robust advantage for non-Hermitian sensing

across all investigated noise regimes. Whether subjected to correlated background noise (Fig. 8a), systematic parameter offsets (Fig. 8b), or detector saturation (Fig. 8c), the FI of the non-Hermitian protocol significantly exceeds that of its Hermitian counterpart. This superiority stems from the interplay between the amplified susceptibility and the distinct scaling of noise contributions.

Specifically, while non-Hermitian protocols offer no intrinsic advantage in the ideal, noiseless QFI limit due to the overhead of Hermitian dilation, they exhibit a transformative benefit in noise-limited regimes. By markedly increasing the “signal” ( $\chi_{\text{nH}} \gg 1$ ) relative to the non-reducible noise floor  $\sigma_{\text{nCLT}}$ , non-Hermitian dynamics effectively shield the parameter information from being buried by hardware imperfections. These findings provide a rigorous information-theoretic foundation for the practical utility of non-Hermitian sensors, corroborating the sensitivity analysis in Sec. III and confirming their resilience even near detector saturation thresholds.

## V. CONCLUSION & OUTLOOK

In conclusion, we have provided a comprehensive analysis of non-Hermitian sensing, focusing on the transition from fundamental quantum limits to practical metrological performance. While recent theoretical findings have underscored that non-Hermitian protocols offer no intrinsic advantage over Hermitian counterparts in the ideal shot-noise-limited regime—once the physical overhead of non-unitary evolution is accounted for—our work demonstrates that this “no-go” conclusion does not extend to realistic experimental settings. Under various technical noise models, we have shown that non-Hermitian platforms can yield significant precision enhancements in the presence of instrumental and environmental imperfections.

The physical origin of this resilience lies in the significantly amplified susceptibility inherent to non-Hermitian dynamics. This mechanism boosts the signal response, allowing it to effectively overcome the constant floor of technical noise, such as readout errors and detector saturation, which often define the operational ceiling in the laboratory. Our results thus reconcile the perceived lack of a universal quantum advantage with the diverse experimental reports of enhanced sensitivity, clarifying that the true value of non-Hermiticity lies in its robustness against practical constraints rather than its scaling in the idealized limit.

Looking forward, our findings open several avenues for future research. Experimentally, the identified noise-resilient regimes provide a concrete roadmap for implementing high-precision sensors in platforms ranging from solid-state spins to superconducting circuits, where technical noise remains a primary bottleneck. Theoretically, extending our framework to multi-parameter estimation and non-Hermitian many-body systems could reveal even more sophisticated strategies for noise suppression. By

shifting the focus toward the functional utility of non-Hermitian physics in realistic environments, this work paves the way for a new generation of sensors that are not only theoretically intriguing but also practically robust in real-world applications.

## VI. ACKNOWLEDGMENTS

This work was supported by the National Natural Science Foundation of China (12425414, 12304572, 12304571), and Quantum Science and Technology-National Science and Technology Major Project (2024ZD0300900, 2024ZD0300902).

- 
- [1] Y. Ashida, Z. Gong, and M. Ueda, Non-Hermitian physics, *Advances in Physics* **69**, 249 (2020).
- [2] E. J. Bergholtz, J. C. Budich, and F. K. Kunst, Exceptional topology of non-Hermitian systems, *Reviews of Modern Physics* **93**, 015005 (2021).
- [3] R. El-Ganainy, K. G. Makris, M. Khajavikhan, Z. H. Musslimani, S. Rotter, and D. N. Christodoulides, Non-Hermitian physics and PT symmetry, *Nature Physics* **14**, 11 (2018).
- [4] C. M. Bender and S. Boettcher, Real spectra in non-Hermitian Hamiltonians having  $\mathcal{PT}$  symmetry, *Phys. Rev. Lett.* **80**, 5243 (1998).
- [5] C. M. Bender, Making sense of non-Hermitian Hamiltonians, *Rep. Prog. Phys.* **70**, 947 (2007).
- [6] C. M. Bender, D. C. Brody, and H. F. Jones, Complex Extension of Quantum Mechanics, *Phys. Rev. Lett.* **89**, 270401 (2002).
- [7] P. Dorey, C. Dunning, and R. Tateo, Spectral equivalences, Bethe ansatz equations, and reality properties in  $\mathcal{PT}$ -symmetric quantum mechanics, *J. Phys. A* **34**, 5679 (2001).
- [8] W. Heiss, Repulsion of resonance states and exceptional points, *Phys. Rev. E* **61**, 929 (2000).
- [9] J. Doppler, A. A. Mailybaev, J. Böhm, U. Kuhl, A. Girschik, F. Libisch, T. J. Milburn, P. Rabl, N. Moiseyev, and S. Rotter, Dynamically encircling an exceptional point for asymmetric mode switching, *Nature* **537**, 76 (2016).
- [10] K. Kawabata, K. Shiozaki, M. Ueda, and M. Sato, Symmetry and topology in non-Hermitian physics, *Phys. Rev. X* **9**, 041015 (2019).
- [11] W. D. Heiss, The physics of exceptional points, *J. Phys. A* **45**, 444016 (2012).
- [12] W. D. Heiss, Exceptional points of non-Hermitian operators, *J. Phys. A* **37**, 2455 (2004).
- [13] J. Wiersig, Prospects and fundamental limits in exceptional point-based sensing, *Nat. Commun.* **11**, 2454 (2020).
- [14] H. Jing, Ş. Özdemir, H. Lü, and F. Nori, High-order exceptional points in optomechanics, *Sci. Rep.* **7**, 1 (2017).
- [15] J. Wiersig, Sensors operating at exceptional points: General theory, *Phys. Rev. A* **93**, 033809 (2016).
- [16] L. Feng, M. Ayache, J. Huang, Y.-L. Xu, M.-H. Lu, Y.-F. Chen, Y. Fainman, and A. Scherer, Nonreciprocal light propagation in a silicon photonic circuit, *Science* **333**, 729 (2011).
- [17] C. E. Rüter, K. G. Makris, R. El-Ganainy, D. N. Christodoulides, M. Segev, and D. Kip, Observation of parity-time symmetry in optics, *Nat. Phys.* **6**, 192 (2010).
- [18] W. Chen, Ş. Kaya Özdemir, G. Zhao, J. Wiersig, and L. Yang, Exceptional points enhance sensing in an optical microcavity, *Nature* **548**, 192 (2017).
- [19] H. Hodaie, A. U. Hassan, S. Wittek, H. Garcia-Gracia, R. El-Ganainy, D. N. Christodoulides, and M. Khajavikhan, Enhanced sensitivity at higher-order exceptional points, *Nature* **548**, 187 (2017).
- [20] L. Feng, Z. J. Wong, R.-M. Ma, Y. Wang, and X. Zhang, Single-mode laser by parity-time symmetry breaking, *Science* **346**, 972 (2014).
- [21] A. Guo, G. J. Salamo, D. Duchesne, R. Morandotti, M. Volatier-Ravat, V. Aimez, G. A. Siviloglou, and D. N. Christodoulides, Observation of  $\mathcal{PT}$ -Symmetry Breaking in Complex Optical Potentials, *Phys. Rev. Lett.* **103**, 093902 (2009).
- [22] M.-A. Miri and A. Alù, Exceptional points in optics and photonics, *Science* **363**, 7709 (2019).
- [23] P. Djorwe, Y. Pennec, and B. Djafari-Rouhani, Exceptional Point Enhances Sensitivity of Optomechanical Mass Sensors, *Phys. Rev. Appl.* **12**, 024002 (2019).
- [24] J. Zhang, B. Peng, Ş. K. Özdemir, K. Pichler, D. O. Krimer, G. Zhao, F. Nori, Y.-x. Liu, S. Rotter, and L. Yang, A phonon laser operating at an exceptional point, *Nat. Photonics* **12**, 479 (2018).
- [25] Z. Zhang, Y. Zhang, J. Sheng, L. Yang, M.-A. Miri, D. N. Christodoulides, B. He, Y. Zhang, and M. Xiao, Observation of Parity-Time Symmetry in Optically Induced Atomic Lattices, *Phys. Rev. Lett.* **117**, 123601 (2016).
- [26] Y. Choi, C. Hahn, J. W. Yoon, and S. H. Song, Observation of an anti-PT-symmetric exceptional point and energy-difference conserving dynamics in electrical circuit resonators, *Nat. Commun.* **9**, 2182 (2018).
- [27] D. Zou, T. Chen, W. He, J. Bao, C. H. Lee, H. Sun, and X. Zhang, Observation of hybrid higher-order skin-topological effect in non-Hermitian topoelectrical circuits, *Nat. Commun.* **12**, 7201 (2021).
- [28] W. Deng, W. Zhu, T. Chen, H. Sun, and X. Zhang, Ultrasensitive integrated circuit sensors based on high-order non-Hermitian topological physics, *Sci. Adv.* **10**, 6905 (2024).
- [29] C. M. Bender, B. K. Berntson, D. Parker, and E. Samuel, Observation of PT phase transition in a simple mechanical system, *J. Phys. A* **81**, 173 (2013).
- [30] Z. Li, L.-W. Wang, X. Wang, Z.-K. Lin, G. Ma, and J.-H. Jiang, Observation of dynamic non-Hermitian skin effects, *Nat. Commun.* **15**, 6544 (2024).
- [31] A. Guo, G. J. Salamo, D. Duchesne, R. Morandotti, M. Volatier-Ravat, V. Aimez, G. A. Siviloglou, and D. N. Christodoulides, Observation of PT-symmetry breaking in complex optical potentials, *Phys. Rev. Lett.* **103**, 093902 (2009).
- [32] J. Ren, H. Hodaie, G. Harari, A. U. Hassan, W. Chow, M. Soltani, D. Christodoulides, and M. Khajavikhan, Ultrasensitive micro-scale parity-time-symmetric ring laser

- gyroscope, *Opt. Lett.* **42**, 1556 (2017).
- [33] N. A. Mortensen, P. A. D. Gonçalves, M. Khajavikhan, D. N. Christodoulides, C. Tserkezis, and C. Wolff, Fluctuations and noise-limited sensing near the exceptional point of parity-time-symmetric resonator systems, *Optica* **5**, 1342 (2018).
- [34] S. Sunada, Large Sagnac frequency splitting in a ring resonator operating at an exceptional point, *Phys. Rev. A* **96**, 033842 (2017).
- [35] S. Bittner, B. Dietz, U. Günther, H. L. Harney, M. Miskioğlu, A. Richter, and F. Schäfer,  $\mathcal{PT}$  Symmetry and Spontaneous Symmetry Breaking in a Microwave Billiard, *Phys. Rev. Lett.* **108**, 024101 (2012).
- [36] C. Dembowski, H.-D. Gräf, H. L. Harney, A. Heine, W. D. Heiss, H. Rehfeld, and A. Richter, Experimental Observation of the Topological Structure of Exceptional Points, *Phys. Rev. Lett.* **86**, 787 (2001).
- [37] Y.-H. Lai, Y.-K. Lu, M.-G. Suh, Z. Yuan, and K. Vahala, Observation of the exceptional-point-enhanced Sagnac effect, *Nature* **576**, 65 (2019).
- [38] L. Bao, B. Qi, D. Dong, and F. Nori, Fundamental limits for reciprocal and nonreciprocal non-Hermitian quantum sensing, *Phys. Rev. A* **103**, 042418 (2021).
- [39] H.-K. Lau and A. A. Clerk, Fundamental limits and non-reciprocal approaches in non-Hermitian quantum sensing, *Nat. Commun.* **9**, 4320 (2018).
- [40] M. Zhang, W. Sweeney, C. W. Hsu, L. Yang, A. Stone, and L. Jiang, Quantum noise theory of exceptional point amplifying sensors, *Phys. Rev. Lett.* **123**, 180501 (2019).
- [41] Y. Chu, Y. Liu, H. Liu, and J. Cai, Quantum sensing with a single-qubit pseudo-Hermitian system, *Phys. Rev. Lett.* **124**, 020501 (2020).
- [42] Z.-P. Liu, J. Zhang, i. m. c. K. Özdemir, B. Peng, H. Jing, X.-Y. Lü, C.-W. Li, L. Yang, F. Nori, and Y.-x. Liu, Metrology with  $\mathcal{PT}$ -Symmetric Cavities: Enhanced sensitivity near the  $\mathcal{PT}$ -phase transition, *Phys. Rev. Lett.* **117**, 110802 (2016).
- [43] W. Langbein, No exceptional precision of exceptional-point sensors, *Phys. Rev. A* **98**, 023805 (2018).
- [44] W. Ding, X. Wang, and S. Chen, Fundamental Sensitivity Limits for Non-Hermitian Quantum Sensors, *Phys. Rev. Lett.* **131**, 160801 (2023).
- [45] X. Yu and C. Zhang, Quantum parameter estimation of non-Hermitian systems with optimal measurements, *Phys. Rev. A* **108**, 022215 (2023).
- [46] C. Chen, L. Jin, and R.-B. Liu, Sensitivity of parameter estimation near the exceptional point of a non-Hermitian system, *New J. Phys.* **21**, 083002 (2019).
- [47] H. Wang, Y.-H. Lai, Z. Yuan, M.-G. Suh, and K. Vahala, Petermann-factor sensitivity limit near an exceptional point in a Brillouin ring laser gyroscope, *Nat. Commun.* **11**, 1610 (2020).
- [48] J. Wiersig, Robustness of exceptional-point-based sensors against parametric noise: The role of Hamiltonian and Liouvillian degeneracies, *Phys. Rev. A* **101**, 053846 (2020).
- [49] Y. Wu, W. Liu, J. Geng, X. Song, X. Ye, C.-K. Duan, X. Rong, and J. Du, Observation of parity-time symmetry breaking in a single-spin system, *Science* **364**, 878 (2019).
- [50] J. Li, A. K. Harter, J. Liu, L. de Melo, Y. N. Joglekar, and L. Luo, Observation of parity-time symmetry breaking transitions in a dissipative Floquet system of ultracold atoms, *Nat. Commun.* **10**, 855 (2019).
- [51] M. Naghiloo, M. Abbasi, Y. N. Joglekar, and K. Murch, Quantum state tomography across the exceptional point in a single dissipative qubit, *Nat. Phys.* **15**, 1232 (2019).
- [52] L. Xiao, Y. Chu, Q. Lin, H. Lin, W. Yi, J. Cai, and P. Xue, Non-Hermitian Sensing in the Absence of Exceptional Points, *Phys. Rev. Lett.* **133**, 180801 (2024).
- [53] Y. Li, C. Liang, C. Wang, C. Lu, and Y.-C. Liu, Gain-Loss-Induced Hybrid Skin-Topological Effect, *Phys. Rev. Lett.* **128**, 223903 (2022).
- [54] N. Zeng, T. Liu, K. Xia, Y.-R. Zhang, and F. Nori, Non-Hermitian sensing from the perspective of postselected measurements, *Phys. Rev. Res.* **7**, 043219 (2025).
- [55] J. C. Budich and E. J. Bergholtz, Non-Hermitian Topological Sensors, *Phys. Rev. Lett.* **125**, 180403 (2020).
- [56] J. Dalibard, Y. Castin, and K. Mølmer, Wave-function approach to dissipative processes in quantum optics, *Phys. Rev. Lett.* **68**, 580 (1992).
- [57] F. Minganti, A. Miranowicz, R. W. Chhajlany, and F. Nori, Quantum exceptional points of non-Hermitian Hamiltonians and Liouvillians: The effects of quantum jumps, *Phys. Rev. A* **100**, 062131 (2019).
- [58] U. Günther and B. F. Samsonov, Naimark-Dilated  $\mathcal{PT}$ -Symmetric Brachistochrone, *Phys. Rev. Lett.* **101**, 230404 (2008).
- [59] K. Kawabata, Y. Ashida, and M. Ueda, Information Retrieval and Criticality in Parity-Time-Symmetric Systems, *Phys. Rev. Lett.* **119**, 190401 (2017).
- [60] J. Naikoo, R. W. Chhajlany, J. Kołodziejki, and A. Miranowicz, Precision assessment in non-Hermitian systems: a comparative study of three formalisms, *New Journal of Physics* **28**, 034508 (2026).
- [61] I. I. Arkhipov, F. Nori, and i. m. c. K. Özdemir, Achieving the Quantum Fisher Information Bound in Pseudo-Hermitian Sensors, *Phys. Rev. Lett.* **136**, 080802 (2026).
- [62] W. D. Heiss, The physics of exceptional points, *J. Phys. A* **45**, 444016 (2012).
- [63] M. V. Berry, Physics of nonhermitian degeneracies, *Czech. J. Phys.* **54**, 1039 (2004).
- [64] W. Ding, X. Wang, and S. Chen, Fundamental sensitivity limits for non-Hermitian quantum sensors, *Phys. Rev. Lett.* **131**, 160801 (2023).
- [65] J. Harris, R. W. Boyd, and J. S. Lundeen, Weak Value Amplification Can Outperform Conventional Measurement in the Presence of Detector Saturation, *Phys. Rev. Lett.* **118**, 070802 (2017).
- [66] M. Huang, R.-K. Lee, L. Zhang, S.-M. Fei, and J. Wu, Simulating Broken  $\mathcal{PT}$ -Symmetric Hamiltonian Systems by Weak Measurement, *Phys. Rev. Lett.* **123**, 080404 (2019).
- [67] J. Naikoo, R. W. Chhajlany, J. Kołodziejki, and A. Miranowicz, Metric formalism for precision assessment in non-Hermitian systems, arXiv preprint arXiv:2506.22571 [quant-ph] (2025), arXiv:2506.22571 [quant-ph].